Supplementary Information for

Curvature fluctuations of fluid vesicles reveal hydrodynamic dissipation within the bilayer

Hammad A. Faizi, Rony Granek, Petia M. Vlahovska

Corresponding Author Petia M. Vlahovska.
E-mail: petia.vlahovska@northwestern.edu

This PDF file includes:

Figs. S1 to S4
Tables S1 to S2
Caption for Movie S1
References for SI reference citations

Other supplementary materials for this manuscript include the following:

Movie S1

1. Flickering spectroscopy: theoretical basis

Fluctuation spectroscopy analyzes the thermally-driven membrane undulations of giant unilamellar vesicles. In essence, a time series of vesicle contours in the focal plane (the equator of the quasi-spherical vesicle) is recorded. The quasi-circular contour is decomposed in Fourier modes,

$$r(\phi,t) = R\sum_{\nu=-\ell_{\max}}^{\ell_{\max}} u_\nu(t)e^{\mathrm{i}\nu\phi} = R\Big(1+\sum_{\ell=0}^{\ell_{\max}}\sum_{m=-\ell}^{\ell} f_{\ell m}(t)Y_{\ell m}(\pi/2,\phi)\Big). \quad [1]$$

where $R=(3V/4\pi)^{1/3}$ is the radius of an equivalent sphere with the volume V of the GUV and ν is the mode number. In practice, $\ell_{\max}$ is the maximum number of experimentally resolved modes. The Fourier coefficient for the ν-th mode is then given by

$$u_\nu(t) = \frac{1}{2\pi R}\int_0^{2\pi} r(\phi,t)e^{-i\nu\phi}d\phi = \sum_{\ell=\nu}^{\ell_{\max}} f_{\ell\nu}(t)n_{\ell\nu}P_{\ell\nu}(0) \quad [2]$$

as all the other terms integrate to zero. In the above equation, we have inserted the definition of the spherical harmonic,

$$Y_{\ell m} = n_{\ell m}P_{\ell m}(\cos\theta)e^{\mathrm{i}m\phi}, \quad n_{\ell m} = \sqrt{\frac{(2\ell+1)(\ell-m)!}{4\pi(\ell+m)!}} \quad [3]$$

where $P_{\ell m}(\cos\theta)$ are the associated Legendre polynomials.

The mean squared amplitude of u_ν is then given by

$$\big\langle|u_\nu|^2\big\rangle = \sum_{\ell=\nu}^{\ell_{\max}}\sum_{\ell'=\nu}^{\ell_{\max}}\big\langle f^*_{\ell'\nu}f_{\ell\nu}\big\rangle n_{\ell\nu}n_{\ell'\nu}P_{\ell\nu}(0)P^*_{\ell'\nu}(0). \quad [4]$$

In terms of the spherical harmonic mode amplitudes, the Helfrich Hamiltonian is given by

$$H = \frac{1}{2}\sum_{\ell,m}(\ell+2)(\ell-1)\Big(\ell(\ell+1)\kappa+\sigma R^2\Big)|f_{\ell m}|^2 \quad [5]$$

showing that indeed all modes are decoupled from each other. Equipartition theorem then dictates

$$\Big\langle f^*_{\ell m}f_{\ell' m'}\Big\rangle = k_BT\Big[(\ell+2)(\ell-1)\Big(\ell(\ell+1)\kappa+\sigma R^2\Big)\Big]^{-1}\delta_{\ell\ell'}\delta_{mm'} \quad [6]$$

Eq. 4 therefore simplifies to

$$\big\langle|u_\nu|^2\big\rangle = \sum_{\ell=\nu}^{\ell_{\max}}\big\langle|f_{\ell\nu}|^2\big\rangle n^2_{\ell\nu}|P_{\ell\nu}(0)|^2 \quad [7]$$

or, explicitly,

$$\big\langle|u_\nu|^2\big\rangle = k_BT\sum_{\ell=\nu}^{\ell_{\max}}\Big[(\ell+2)(\ell-1)\Big(\ell(\ell+1)\kappa+\sigma R^2\Big)\Big]^{-1}n^2_{\ell\nu}|P_{\ell\nu}(0)|^2 \quad [8]$$

A. Autocorrelation function of the equatorial plane Fourier modes: Asymptotic behavior for tensionless membranes. The auto-correlation function (ACF) of the equatorial plane Fourier modes is given by

$$\Big\langle u_\nu(0)u^*_\nu(t)\Big\rangle = \sum_{\ell=|\nu|}^{\ell_{max}} A_{\ell\nu}e^{-\omega(\ell)\,t} \quad [9]$$

where for $\omega(\ell)$ we shall use here Eq. (32) (see explanation in the main text for its validity for GUVs dynamics), and

$$A_{\ell\nu} = \Big\langle|f_{\ell\nu}|^2\Big\rangle n^2_{\ell\nu}\Big|P_{\ell\nu}(0)\Big|^2. \quad [10]$$

Let us consider the short and long time asymptotic behaviors of the ACF. At times t much longer than the longest relaxation time of Eq. (31), $\omega(\nu)^{-1}$, the ACF reduces to a single exponential relaxation

$$\Big\langle u_\nu(0)u^*_\nu(t)\Big\rangle \simeq A_{\nu\nu}e^{-\omega(\nu)\,t} \quad [11]$$

For short times, $t\ll\omega(\nu)^{-1}$, we consider the $\ell\gg1$ behavior of the series terms, and approximately evaluate the series by transforming it to an integral. For $\ell\gg\nu$, we have from Eq. (3) $n^2_{\ell\nu}\simeq\ell^{1-2\nu}/(2\pi)$, and the associate Legendre polynomials behave as (1)

$$P_{\ell\nu}(\cos\theta)\simeq\frac{2}{\sqrt{\pi}}\frac{\Gamma[\ell+\nu+1]}{\Gamma[\ell+3/2]}\frac{\cos\left[(\ell+1/2)\theta-\pi/4+\nu\pi/2\right]}{\sqrt{2\sin\theta}}+o(1/\ell) \quad [12]$$

such that for $\theta = \pi/2$ and $\ell \gg \nu$ we obtain

$$P_{\ell\nu}(0) \simeq \sqrt{\frac{2}{\pi}}\, \ell^{\nu-1/2} \cos\left[(\ell+\nu)\pi/2\right]$$

or

$$P_{\ell\nu}(0) \simeq \sqrt{\frac{2}{\pi}}\, \ell^{\nu-1/2} \times \begin{cases} 0 & \ell+\nu \text{ is odd} \\ (-1)^{(\ell+\nu)/2} & \ell+\nu \text{ is even} \end{cases} \quad [13]$$

These lead to

$$n_{\ell\nu}^2 P_{\ell\nu}(0)^2 \simeq \frac{1}{\pi^2} \times \begin{cases} 0 & \ell+\nu \text{ is odd} \\ 1 & \ell+\nu \text{ is even} \end{cases} \quad [14]$$

and the sum in Eq. (31) becomes

$$\left\langle u_\nu(0) u_\nu^*(t) \right\rangle = \frac{1}{\pi^2} \sum_{\ell=|\nu|,2}^{\ell_{max}} \left\langle |f_{\ell\nu}|^2 \right\rangle e^{-\omega(\ell)\, t} \quad [15]$$

Transforming the sum to an integral leads to

$$\left\langle u_\nu(0) u_\nu^*(t) \right\rangle = \frac{1}{2\pi^2} \int_{\ell=|\nu|}^{\ell_{max}} d\ell \left\langle |f_{\ell\nu}|^2 \right\rangle e^{-\omega(\ell)\, t} \quad [16]$$

(The prefactor of 1/2 arises because in Eq. (14) the sum is with interval 2.) Finally, we can use in Eq. (16) the large ℓ limits of $f_{\ell\nu}$ and $\omega(\ell)$, *with the tension being neglected*, and assuming $\chi_s \gg 1$

$$\left\langle |f_{\ell\nu}|^2 \right\rangle \simeq \frac{k_B T}{\kappa \ell^4} \quad [17]$$

and

$$\omega(\ell) \approx \begin{cases} \frac{\kappa}{4\chi_s \eta R^3}\, \ell^4 & 1 \ll \ell \ll \chi_s \\ \frac{\kappa}{4\eta R^3}\, \ell^3 & \chi_s \ll \ell \ll \ell_{max} \end{cases} \quad [18]$$

Thus, for $\nu \gg 1$ the variance of the equatorial Fourier modes (i.e., the static, $t = 0$, ACF) is evaluated to give

$$\left\langle |u_\nu|^2 \right\rangle \simeq \frac{1}{6\pi^2} \frac{k_B T}{\kappa \nu^3} \quad [19]$$

which shows the known $\sim \nu^{-3}$ scaling (2, 3). Furthermore, in this large ν limit, $C_\nu \equiv A_{\nu\nu} / \left\langle |u_\nu|^2 \right\rangle$ is a slowly decreasing function of ν that can be well presented by $C_\nu \simeq 0.66 \ln \nu / \nu^{1/2}$, determining the ratio of the surviving ACF exponential relaxation amplitude to the initial ACF (i.e., static) value.

We now wish to replace the lower bound of the integral in Eq. (16) by 0, however, since the integral diverges as the lower bound approaches 0, we make use of the identity

$$\left\langle u_\nu(0) u_\nu^*(t) \right\rangle = \left\langle |u_\nu|^2 \right\rangle - \frac{1}{2\pi^2} \int_{\ell=|\nu|}^{\ell_{max}} d\ell \left\langle |f_{\ell\nu}|^2 \right\rangle \left(1 - e^{-t\omega(\ell)}\right) \quad [20]$$

Note that the second integral is essentially half of the MSD of the ν-th Fourier mode, $\langle \Delta u_\nu(t)^2 \rangle \equiv \langle (u_\nu(t) - u_\nu^*(0))^2 \rangle$.

"Scaling" the integral in Eq. (20) (i.e. changing the variable of integration), we obtain the two "short times" regimes, commencing by a solvent viscosity dominated regime which is followed by a membrane viscosity dominated regime. The crossover time separating the two regimes is

$$t^* \approx \frac{4\eta R^3}{\kappa \chi_s^3}\ . \quad [21]$$

For the earlier regime of "short times", $t_0 \ll t \ll t^*$, where t_0 is the shortest relaxation time, $t_0 = 1/\omega(\ell_{max})$, we get the solvent dissipation regime

$$\left\langle u_\nu(0) u_\nu^*(t) \right\rangle \simeq \left\langle |u_\nu|^2 \right\rangle - \frac{1}{8\pi^2} \frac{k_B T}{\eta R^3}\, t \left[\frac{1}{3} \ln\left(\frac{4\eta R^3}{\kappa \nu^3\, t} \right) + 0.2838 \right] \quad [22]$$

For the late regime of "short times", $t^* \ll t \ll \omega(\nu)^{-1}$, we obtain the membrane dissipation regime

$$\left\langle u_\nu(0) u_\nu^*(t) \right\rangle \simeq \left\langle |u_\nu|^2 \right\rangle - \frac{\Gamma[1/4]}{6\pi^2} \frac{k_B T}{\kappa} \left(\frac{\kappa}{4\chi_s \eta R^3}\, t \right)^{3/4} \quad [23]$$

presenting a non-exponential relaxation of the ACF from its static value; effectively (to first order) it is a stretched exponential decay with stretching exponent 3/4. Equivalently, the amplitude of the equatorial Fourier mode ν is anomalously diffusing with exponent 3/4, since its MSD is equal to $2\left(\langle |u_\nu|^2 \rangle - \langle u_\nu(0) u_\nu^*(t) \rangle\right)$. This exponent also describes the short-time (polymer segment) anomalous diffusion of semi-flexible polymers obeying the worm-like chain model (4, 5).

B. Transverse Mean Squared displacement of a membrane segment for tensionless membranes: Implications for the Dynamic Structure Factor. In Refs. (5–8) it was shown that pure bending undulations, that are dissipated by solvent viscosity, produce a transverse subdiffusion of a membrane segment with a mean squared displacement (MSD) that grows in time as $t^{2/3}$. At large scattering wavenumbers k that are sensitive to single membrane dynamics, this subdiffusion leads to stretched exponential relaxation, $\sim \mathrm{Exp}\left[-(\Gamma_k t)^{2/3}\right]$, of the dynamic structure factor (DSF) of membrane phases (6–9). We now discuss how these dynamics are modified when membrane viscosity is included.

B.1. Mean Square Displacement of a membrane segment. The dimensionless membrane segment MSD at an arbitrary 3D angle $\Omega = (\theta, \phi)$, $\langle(\Delta f(t))^2\rangle \equiv \langle(f(\Omega,t) - f(\Omega,0))^2\rangle$, is given by (note that the MSD with physical dimensions is given by $\langle(\Delta h(t))^2\rangle \equiv R^2\langle(\Delta f(t))^2\rangle$)

$$\langle(\Delta f(t))^2\rangle = 2k_BT\sum_{\ell=2}^{\ell_{\max}}\sum_{m=-\ell}^{\ell}|Y_{\ell m}(\Omega)|^2\left[(\ell+2)(\ell-1)\Big(\ell(\ell+1)\kappa+\sigma R^2\Big)\right]^{-1}\left(1-e^{\omega(\ell)\,t}\right) \quad [24]$$

Using

$$\sum_{m=-l}^{l}|Y_{\ell m}(\Omega)|^2 = \frac{2l+1}{4\pi} \quad [25]$$

(which may be verified by using Eq. 3), we arrive at

$$\langle(\Delta f(t))^2\rangle = \frac{k_BT}{2\pi}\sum_{\ell=2}^{\ell_{\max}}(2l+1)\left[(\ell+2)(\ell-1)\Big(\ell(\ell+1)\kappa+\sigma R^2\Big)\right]^{-1}\left(1-e^{-\omega(\ell)\,t}\right) \quad [26]$$

which is independent of the angle Ω as expected.

We now assume again *vanishing tension*. For times $t_0 \ll t \ll \tau_R$, where t_0 and τ_R are the shortest and longest relaxation times (respectively), $t_0 \equiv 1/\omega(\ell_{max})$ and $\tau_R \equiv 1/\omega(2)$, we may use the $\ell \gg 1$ asymptotic of both the spectrum of modes ($\sim \ell^{-4}$) and of the relaxation frequency $\omega(\ell)$, as given by Eq. (18), and use $2\ell+1 \simeq 2\ell$. We may also replace the sum in Eq. (26) by an integral, with the lower and upper integration limits replaced by 0 and ∞, respectively. This leads to

$$\langle(\Delta f(t))^2\rangle \simeq \frac{k_BT}{\pi\kappa}\int_0^\infty d\ell\,\ell^{-3}\left(1-e^{-\omega(\ell)t}\right) \quad [27]$$

Note that the latter expression is identical to the one derived for flat membranes using standard 2D Fourier modes (6, 7), yet for flat membranes $\chi_s = 0$ by definition.

Eq. (27) leads to two "short time" regimes, a solvent viscosity dominated regime that is followed by a membrane viscosity dominated regime. We find

$$\langle(\Delta h(t))^2\rangle \equiv R^2\langle(\Delta f(t))^2\rangle \approx \begin{cases}\frac{\Gamma[1/3]}{2\pi 4^{2/3}}\frac{k_BT}{\eta^{2/3}\kappa^{1/3}}\,t^{2/3} & t_0 \ll t \ll t^* \\ \frac{1}{4\sqrt{\pi}}\frac{k_BTR}{\sqrt{\kappa\eta_m}}\,t^{1/2} & t^* \ll t \ll \tau_R\end{cases} \quad [28]$$

Importantly, $\frac{\tau_R}{t^*} \approx \chi_s^4$, which allows for a very wide membrane viscosity dominated regime if $\chi_s \gg 1$.

B.2. Dynamic Structure Factor. Following Refs. (6–9), the membrane segment MSD controls the DSF relaxation. Excluding the effect of center-of-mass diffusion, which comes in the form of a multiplying factor, and for polydisperse and (sufficiently) large vesicles – as described in detail in Ref. (8) – the main DSF relaxation is well captured by

$$S(k,t) \sim \mathrm{Exp}[-\frac{k^2}{2}\langle(\Delta h(t))^2\rangle]\,.$$

$\langle(\Delta h(t))^2\rangle$ is calculated above, for the case of a membrane with relaxed lipid density. Our analysis of the fluctuations of a quasi-spherical vesicles shows that in principle the Zilman-Granek (ZG), i.e., bulk viscosity dominated, decay, should be followed by a new, membrane viscosity dominated, decay, as follows

$$S(k,t) \approx S(k) \times \begin{cases}\mathrm{Exp}[-(\Gamma_k^{(b)}t)^{2/3}] & t_0 \ll t \ll t^* \\ \mathrm{Exp}[-(\Gamma_k^{(m)}t)^{1/2}] & t^* \ll t \ll \tau_R\end{cases} \quad [29]$$

where $\Gamma_k^{(b)}$ is the ZG relaxation rate (possibly with $\tilde{\kappa}$ replacing κ (9)), and the new, membrane viscosity controlled, relaxation rate, is given by

$$\Gamma_k^{(m)} \simeq \frac{(k_BT)^2R^2}{64\pi\kappa\eta_m}k^4 \quad [30]$$

Given that t^* can be extremely short for viscous membrane vesicles with $R \sim 20-50$ nm, it is quite possible that the whole NSE time range is controlled by membrane viscosity. Moreover, lipid density fluctuations may influence the dynamics probed by NSE (9). Further efforts are required to include other important effects associated with small vesicle sizes.

2. Flickering spectroscopy: experiment

Flickering spectroscopy has become a popular technique to extract out membrane rigidity and tension due to its non-intrusive nature and well developed statistical analysis criteria. The methodology is detailed in (3, 10, 11). To summarize, a time series of the equatorial contour of a giant quasi-spherical vesicle ($R \sim 10\,\mu$m) is recorded using phase-contrast microscopy and high-speed camera. The quasi-circular contour is decomposed in Fourier modes, $r_s(\phi, \pi/2, t) = R\sum u_\nu e^{-\mathrm{i}\nu\phi}$. The autocorrelation function (ACF) of the Fourier modes of the equatorial cross-section picks up all the $m = \nu$ terms of the expansion of the vesicle shape $r_s(\phi, \pi/2, t)$ in spherical harmonics, see Eq. 1, leading to an ACF in the form

$$\mathrm{ACF}(t) = \langle u_\nu(0)u_\nu^*(t)\rangle = \sum_{\ell=|\nu|}^{\ell_{max}} \frac{k_BT}{\kappa\left((\ell-1)(\ell+2)\left(\ell(\ell+1)+\sigma\right)\right)} n_{\ell\nu}^2 \left|P_{\ell\nu}(1)\right|^2 e^{-\omega(\ell)t} \qquad [31]$$

where where k_BT is the thermal energy (k_B is the Boltzmann constant and T is the temperature) and $P_{\ell\nu}$ is the associate Legendre polynomial, see Eq. 3. κ is the bending rigidity and $\bar{\sigma} = \sigma R^2/\kappa$ is the reduced membrane tension. The relaxation rate is

$$\omega(\ell, \kappa, \chi_s) = \frac{\kappa}{\eta R^3} \frac{(\ell-1)\ell(\ell+1)(\ell+2)\left(\ell(\ell+1)+\bar{\sigma}\right)}{4\ell^3+6\ell^2-1+\left(4\ell^2+4\ell-8\right)\chi_s}\,, \qquad [32]$$

where $\chi_s = \eta_m/R\eta$ is a dimensionless membrane viscosity parameter, the ratio of the Saffman-Delbrück length (η_m/η) to the vesicle radius R.

The bilayer elastic properties, bending rigidity and tension, are obtained from the variance of the shape fluctuations (Eq. 31 at $t = 0$). The resulting spectrum is shown in Fig. 1b in the main text. Rescaling the variance by the bending rigidity κ collapses the data, see Fig. 1c in the main text, confirming that the static spectrum is dominated by the bending rigidity.

Figure S1a illustrates the behavior of the ACF of undulations with different wavelengths. The relaxation rate increases with mode number (or equivalently decreases with undulation wavelength), see Figure S1c, and the corresponding ACF decays faster. The membranes viscosity decreases the relaxation rate and slows down the ACF decay, see Figure S1b. Note that the experimentally obtained ACF may show a drop between the first two time points due to experimental white noise, see inset in Figure S1a, however this does not affect the decay of the ACFs. Accordingly, all ACFs are normalized by its value immediately after $t = 0$.

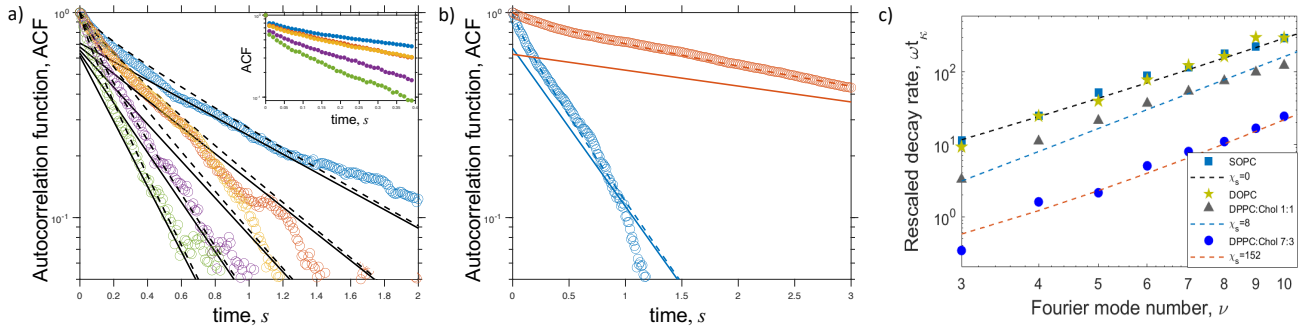

Fig. S1. (a) Autocorrelation functions (ACF) as a function of time (in seconds) for Fourier modes 4-8 of the fluctuating equatorial contour of vesicles made of PS0. Inset: The raw data for the ACF at short times. (b) The ACF of the 6th mode of vesicles made of low viscosity PS0 ($\chi_s = 0$) and high viscosity PS1 ($\chi_s = 50$) diblock-copolymer bilayer membranes. Solid lines correspond to the single-exponential long-time behavior, dashed line correspond to the full expression Eq. 31. (c) The long-time single exponential decay rate obtained from the ACF of the phsopholipid DPPC:DOPC membranes as a function of the mode number. Dashed line is the theory Eq. 32.

The integration time effect of the camera is minimized by acquiring images at a low shutter speed of 200 μs. Images are acquired with SA1.1 high speed camera (Photron) at 50-500 fps for 5-10 mins for a total of 0.1-0.5 million images. Only vesicles with low tension value in the range $10^{-8} - 10^{-10}$ N/m are chosen. This results in a small cross over mode given by $\nu_c = \sqrt{\bar{\sigma}}$ above which the shape fluctuations are dominated by bending rigidity. The ellipsoidal mode (ν =2) has been ignored from the analysis as it is weighted with most excess area which leads to fluctuations with an increased amplitude.

Correctly resolving the dynamics, especially at long wavelengths, where the effect of the membrane viscosity is expected, requires good statistics. There are two important time scales that affect the quality of the analysis. The first is $t_{\max}$, the duration of the recording. The second is the time step in the time series, Δt, which experimentally corresponds to the frames per second (fps) or acquisition speed of the movie. $t_{\max}$ is related to the slowest relaxation mode corresponding to $\ell = 2$ (long wavelength curvature fluctuations (smaller mode numbers) take long time to explore their configurations), while Δt is determined by the highest experimentally resolved mode $\ell = \nu_{\max}$. We found that a factor of 10 ensures good statistics and converged results. $t_{\max} = 10\omega^{-1}(\ell = 2)\,, \quad \Delta t = 1/10\omega^{-1}(\ell = \nu_{\max})$, where ω is given by Eq. 32.

Figure S2 illustrates the importance of collecting long enough data set to ensure good statistics for the equilibrium spectrum. Figure S2a shows a typical SOPC fluctuation equilibrium spectrum determined from data taken over 300 seconds ($t_{\max} = 37$ s). If the same data is trimmed shorter time, e.g., the first 150 seconds only, the same spectrum is recovered. This implies that

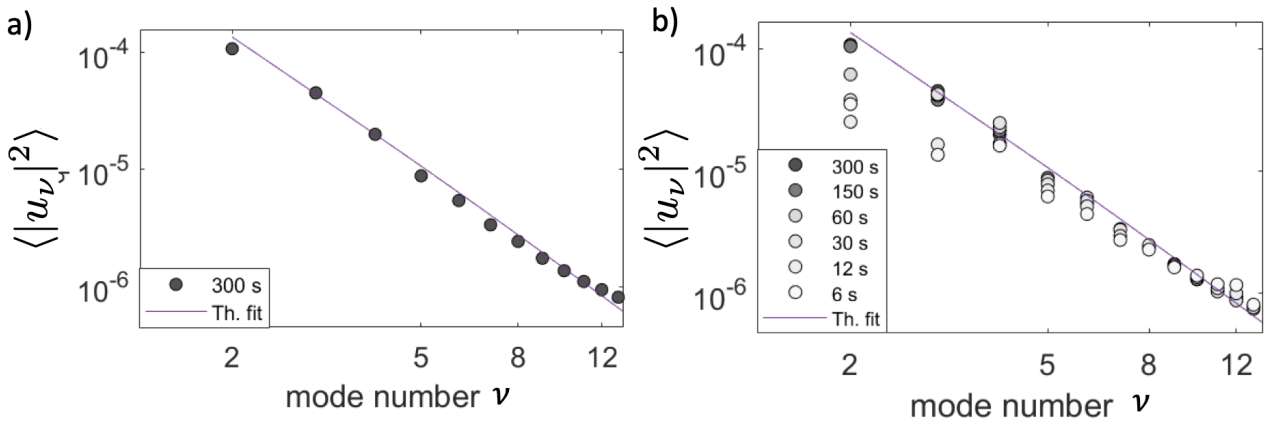

Fig. S2. (a) Equilibrium fluctuation spectrum of SOPC taken over a data set of 300 seconds. b) The same data set is trimmed to first 150, 60, 30, 12, 6 seconds. For this system $\chi_s \sim 0$ and $t_{\max} = 37$s, $\Delta t = 0.0034$s, which corresponds to 294fps. Solid line is the theoretical fit with the static spectrum (Eq. 31 at $t = 0$).

experimental convergence has been achieved. However, trimming the data to the first 60 seconds, or shorter, results in artifacts starting from lower mode number spectrum and creeping to higher ones. The spectrum can be misinterpreted with a higher tension value. This demonstrates the importance of having data with good and sufficient temporal statistics.

Table S1. Computed $t_{\max}$ and Δt for membranes with varying dimensionless membrane viscosity, χ_s. Other parameters assumed are $\kappa = 25 k_B T$, $R = 10\,\mu m$, $\eta = 10^{-3}$ Pa.s, $\sigma = 0$. These numbers were also chosen for experiments as well.

Membrane Viscosity	$t_{relax,2}$ (s)	$t_{\max}$ (s)	$t_{relax,10}$ (s)	Δt (s)	fps
$\chi_s = 0$	3.7	37	0.034	0.0034	294
$\chi_s = 1$	4.8	48	0.037	0.0037	270
$\chi_s = 10$	14.5	145	0.067	0.0067	149
$\chi_s = 100$	112	1120	0.36	0.036	27

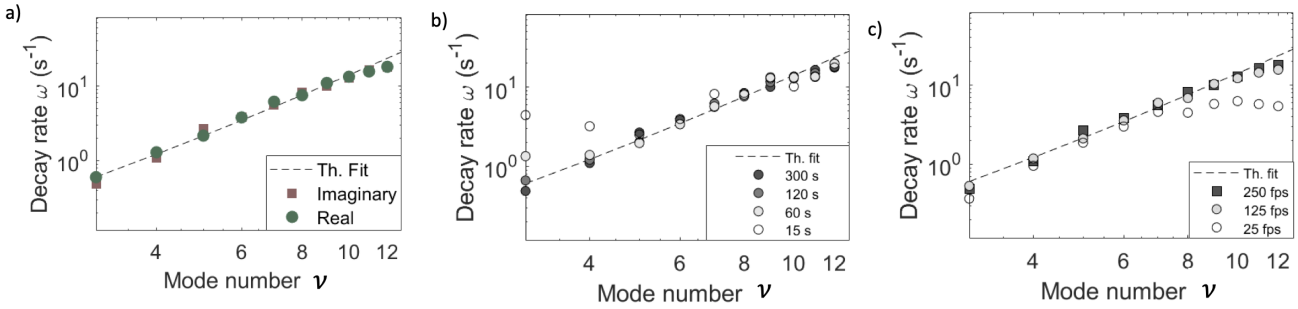

Fig. S3. (a) Decay rate obtained from both imaginary and real parts of the Fourier modes for a SOPC vesicle with $\chi_s < 1$. The experiment was conducted for 300 secs. b) The same data set is trimmed to first 120, 60, 15 seconds at 250 fps. c) The same data set taken for 300 seconds but evaluated at different fps.

For time correlations analysis of the same vesicle as in Fig. S2a, Figure S3 illustrates the importance of time scales $t_{\max}$ and Δt. Analyzing the data for a trimmed data set results in artifacts in data interpretation at lower modes as shown in Figure S3b with a higher membrane tension. Similarly, analyzing the data set at lower fps or lower temporal resolution affects higher mode number data as shown in S3b. It can been seen that the artifacts exacerbate for membranes with higher membrane viscosity like DPPC:Chol (1:1) with $\chi_s \sim 10$ as shown by time correlation analysis in Figure S4.

Increasing the membrane viscosity slows down the dynamics and requires recording vesicle fluctuations over longer times to achieve good statistics. The power-spectrum of DPPC:Chol (1:1) membrane which has with $\chi_s \sim 10$ is shown in Fig. S4a. The time correlations analysis is also very sensitive to the data quality. Fig. S4b. shows that insufficient data give rise to artificial increase in the decay rates of the lower wave-number modes. Analyzing the data set at lower fps or lower temporal resolution affects the decay rates, of the higher modes, see Fig. S4c.

Table S2 summarizes the material properties of the bilayer membranes

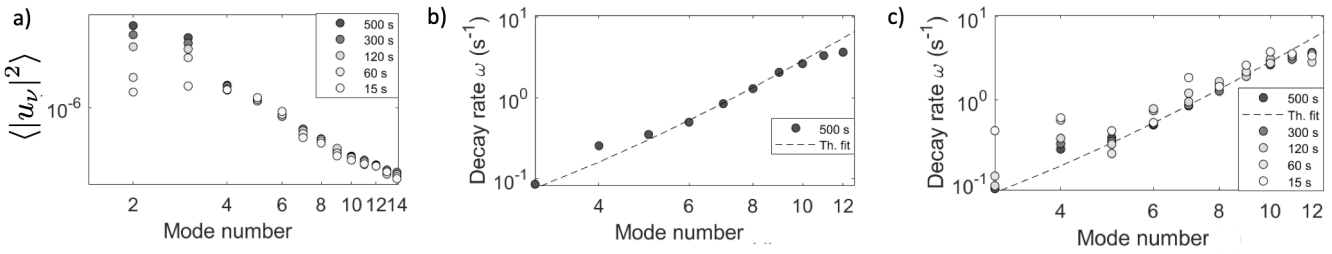

Fig. S4. a) Equilibrium fluctuation spectrum of DPPC:Chol (1:1) taken over a data set of 500 seconds. b) Decay rate obtained for the same vesicle in a) with $\chi_s \sim 10$ c) The same data set is trimmed to first 300, 120, 60, 15 seconds at 250 fps.

Table S2. **Membrane bending rigidity and viscosity for various bilayer systems at 25.0 ^{o}C. L_d and L_o refer to liquid-disordered and liquid-ordered phases respectively. FA refers to fluctuation analysis and ED refers to Electrodeformation. χ_s is computed for GUV with radius 10 μm in solution with viscosity 10^{-3} Pa.s.m using the membrane viscosity from ED. The data for the bending rigidity and ED viscosity for the PS systems are from (12).**

Composition	Bending Rigidity κ	Viscosity η_m, ED	Viscosity η_m, FA	χ_s
	(k_BT)	(nPa.s.m)	(n.Pa.s.m)	$=\eta_m/\eta R$
DOPC	21.7$\pm$3.1	4.1$\pm$2.6	not detectable	0.4
SOPC	25.7$\pm$3.6	9.7$\pm$3.0	not detectable	1.0
DPPC:Chol (1:1)	124.4$\pm$14.0	57.6$\pm$12.6	89.7$\pm$26.3	5.8
DPPC:Chol (6:4)	152.6$\pm$12.6	83.6$\pm$14.3	106$\pm$47	8.4
DPPC:Chol (7:3)	189.6$\pm$17.0	1450$\pm$928	1777$\pm$682	145
PBd_{13}-*b*-PEO_{11} (PS0)	17.1$\pm$1.5	14.4 ± 4.40	not detectable	1.4
PBd_{22}-*b*-PEO_{14} (PS1)	31.0$\pm$5.1	686 ± 51.0	variable	68.6

Movie S1. Thermally-driven shape fluctuations of a giant vesicle (radius 21 μm) observed with a phase contrast microscopy. Magnification 40x.

References

1. I. S. Gradshteyn and I. M. Ryzhik. *Table of Integrals, Series, and Products: pp. 1003, Sec. 8.72, item 3, ref. (MO 92)*. Academic Press, New York, 1980.
2. J. Pecreaux, H.-G. Dobereiner, J. Prost, J.-F. Joanny, and P. Bassereau. Refined contour analysis of giant unilamellar vesicles. *Eur. Phys. J. E.*, 13:277–290, 2004.
3. R. S. Gracia, N. Bezlyepkina, R. L. Knorr, R. L. Lipowsky, and R. Dimova. Effect of cholesterol on the rigidity of saturated and unsaturated membranes: fluctuation and electrodeformation analysis of giant vesicles. *Soft Matter*, 6:1472 – 1482, 2010.
4. Emmanuel Farge and Anthony C. Maggs. Dynamic scattering from semiflexible polymers. *Macromolecules*, 26(19): 5041–5044, 1993. . URL https://doi.org/10.1021/ma00071a009.
5. R Granek. From semi-flexible polymers to membranes: Anomalous diffusion and reptation. *J. Physique II*, 7(12):1761–1788, DEC 1997. ISSN 1155-4312.
6. A. G. Zilman and R. Granek. Undulations and dynamic structure factor of membranes. *Phys. Rev. Lett.*, 77:4788–4791, Dec 1996. . URL https://link.aps.org/doi/10.1103/PhysRevLett.77.4788.
7. Anton G. Zilman and Rony Granek. Membrane dynamics and structure factor. *Chemical Physics*, 284(1):195–204, 2002. ISSN 0301-0104. . URL https://www.sciencedirect.com/science/article/pii/S0301010402005487. Strange Kinetics.
8. Rony Granek, Ingo Hoffmann, Elizabeth G. Kelley, Michihiro Nagao, Petia M. Vlahovska, and Anton Zilman. Dynamic structure factor of undulating vesicles: finite-size and spherical geometry effects with application to neutron spin echo experiments. *EUROPEAN PHYSICAL JOURNAL E*, 47(2), FEB 2024. ISSN 1292-8941. .
9. M. C. Watson, Y. Peng, Y. Zheng, and F. L. H. Brown. The intermediate scattering function for lipid bilayer membranes: From nanometers to microns. *J. Chem. Phys.*, 135:194701, 2011.
10. Hammad A. Faizi, Shelli L. Frey, Jan Steinkuehler, Rumiana Dimova, and Petia M. Vlahovska. Bending rigidity of charged lipid bilayer membranes. *Soft Matter*, 15(29):6006–6013, AUG 7 2019. ISSN 1744-683X. .
11. Hammad A. Faizi, Cody J. Reeves, Vasil N. Georgiev, Petia M. Vlahovska, and Rumiana Dimova. Fluctuation spectroscopy of giant unilamellar vesicles using confocal and phase contrast microscopy. *Soft Matter*, 16:8996–9001, 2020. . URL http://dx.doi.org/10.1039/D0SM00943A.
12. Hammad A. Faizi, Rumiana Dimova, and Petia M. Vlahovska. A vesicle microrheometer for high-throughput viscosity measurements of lipid and polymer membranes. *BIOPHYSICAL JOURNAL*, 121(6):910–918, MAR 15 2022. ISSN 0006-3495. .